






Received 28 June 2020; revised 13 August 2020 and 11 October 2020; accepted 18 November 2020. Date of publication 27 November 2020; date of current version 14 December 2020. The review of this article was arranged by Associate Editor Luigi Martirano.

Digital Object Identifier 10.1109/OJIA.2020.3041209

Utilization of Supercapacitor to Extend the Critical Clearing Time in a Power System

TALITHA P. SARI ¹ (Student Member, IEEE), JINHO KIM ³ (Member, IEEE),
ARDYONO PRIYADI¹ (Member, IEEE), VITA LYSTIANINGRUM ¹ (Member, IEEE),
MAURIDHI H. PURNOMO ² (Senior Member, IEEE), AND EDUARD MULJADI ³ (Fellow, IEEE)

(Invited Paper)

¹Department of Electrical Engineering, Institut Teknologi Sepuluh Nopember, Surabaya 60111, Indonesia

²Department of Electrical Engineering, Computer Engineering, and University Center of Excellence on Artificial Intelligence for Healthcare and Society (UCE AIHeS), Institut Teknologi Sepuluh Nopember, Surabaya 60111, Indonesia

³Department of Electrical and Computer Engineering, Auburn University, Auburn, AL 36849 USA

CORRESPONDING AUTHOR: MAURIDHI H. PURNOMO (e-mail: hery@ee.its.ac.id)

This work was supported in part by Indonesian Ministry of Research and Higher Education, under “Pendidikan Magister menuju Doktor untuk Sarjana Unggul (PMDSU)” scholarship.

ABSTRACT Future power systems with a high penetration level of inverter-based renewable sources (IBRSs) will be vulnerable to severe grid faults because of the noticeable reduction in the total system inertia. Particularly, challenges will arise in securing the transient stability limits of synchronous generators in the systems. Fortunately, the stability limits can be extended by utilizing the existing inverter-based units as virtual damping devices. This paper proposes the utilization of an inverter-based supercapacitor (IBSC) to extend the critical clearing time (CCT) of a power system with a high penetration level of IBRSs; thus, it makes it possible to secure the transient stability limits of SGs. In order to utilize an IBSC, the controllability of the IBSC is explored by considering two factors: control scheme and location of the IBSC. First, to determine an effective control scheme for the IBSC, three control schemes, which are power-damping control, speed-damping control, and power and speed-damping control, are tested under severe fault conditions. Then, using each control scheme, the location of the IBSC is chosen in a certain power system by the most extended CCT. The proposed utilization strategy was validated under various scenarios in a modified IEEE 14-bus system using the PSCAD simulator.

INDEX TERMS Angle stability, critical clearing time, damping, fault location, oscillation, supercapacitor.

I. INTRODUCTION

Renewable energy resources have been increasing in an effort to reduce fossil fuel consumption [1], [2]. In addition, the accommodation of inverter-based renewable sources (IBRSs) is increasing to enhance the generation efficiency of renewable sources. However, the increasing penetration level of IBRSs will arise an issue in the transient stability by causing noticeable reductions in the fault contribution and the total system inertia [3]. The reduction in the fault contribution will make it difficult to diagnose grid faults by detecting the fault currents; therefore, there might be a failure to discern the fault or a delay in the relay operation, and synchronous generators (SGs) near the fault might exceed their stability

limits. In addition, the reduced system inertia will deteriorate the system performance during a fault, and even after the fault clearance by making the generators swing severely; in the end, it can cause loss of synchronism. Loss of synchronism can sufficiently lead to system blackout [4], [5]. In order to secure stability limit of SGs in a power system with a high penetration level of IBRSs, the critical clearing time (CCT), the maximum time during which a disturbance can be applied without the system losing its stability, has to be extended.

Regarding the issue mentioned above, many studies have proposed control strategies [6]–[12] to improve the transient stability limit of power systems. In [6], [7], a switching control strategy for the power system stabilizer (PSS) was proposed

to mitigate the oscillated operation of an applicable SG. This control strategy needs to consider interactions among the SGs to be applied to a power system consisting of multiple SGs. In [8], a passive-resistive load was used to damp out the oscillation of SGs in a power system. The performance of this strategy was limited by the size of the load.

In [9]–[12], energy storage systems (ESSs) were utilized to extend the stability limits of SGs in a power system. In [9], a generic battery storage model was used to regulate the speed of a SG at a constant by repeating charging and discharging according to the speed after a grid fault. This strategy shows the potential of ESSs in securing the angle stability of a SG. In [10], a combination of superconducting magnetic energy storages (SMESs) and superconducting fault current limiters (SFCLs) was proposed to improve the angle stabilities of SGs in a power system. The SFCL has a resistor that operates during a fault to limit the fault current and reduces the voltage dip at the SMES. Thus, SMES is able to provide a damping control effectively. However, to achieve the strategy in [10], a set of a SFCL and a SMES are required.

An inverter-based supercapacitor (IBSC) was utilized to provide the damping control, and its performance was compared with SMES [11]. It shows that an IBSC has a better performance in damping the oscillation of a SG than that of SMES. However, the control strategy in [11] need to be tested by considering the interactions among the SGs. In [12], a model predictive control was proposed to coordinate multiple ESSs to damp out the rotor angles of multiple SGs. However, the locations of the ESSs were assumed to be predetermined, and thus various locations of the ESSs are needed to be explored to determine its locations for the damping control.

This paper proposes the utilization of an inverter-based supercapacitor (IBSC) to extend the CCT of a power system with a high penetration level of IBRSs; thus, it can secure the transient stability limits of SGs. In order to utilize an IBSC, the controllability of the IBSC is explored by considering two factors: control scheme and location of the IBSC. First, to determine an effective control scheme for the IBSC, three control schemes, which are power-damping control, speed-damping control, and power and speed-damping control, are tested under severe fault conditions. Then, using each control scheme, the location of the IBSC is chosen in a certain power system by the most extended CCT. The proposed utilization strategy was validated under various scenarios in a modified IEEE system using PSCAD simulator [13].

The remainder of this paper is organized as follows. Determination and effect of extended CCT in power system in Section II. Utilization of SCES is presented in Section III. Simulation results of several cases studies are given in Section IV, and conclusions are given in Section V.

II. DETERMINATION OF CCT & EFFECT OF EXTENDED CCT IN POWER SYSTEMS

The high penetration of IBRSs is affecting the stability system, especially the transient stability. The transient stability index is measured through CCT. Furthermore, the effect of

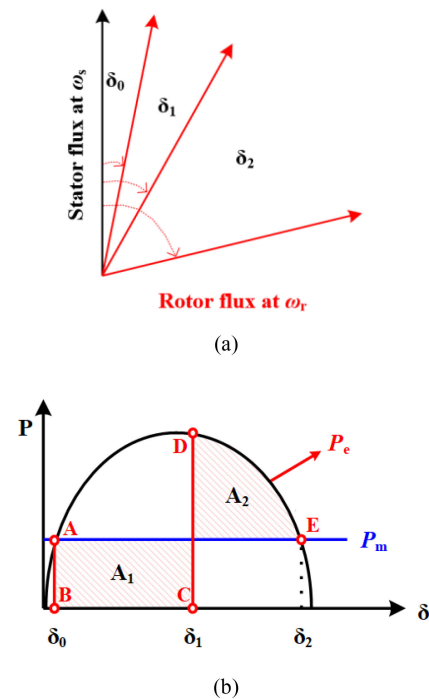


FIGURE 1. Dynamics of a SG for a short circuit. (a) Rotor flux dynamics of a SG. (b) P - δ curve of a SG.

IBSCs in the power system is studied to enhance transient stability. This section describes the determination of CCT and the effect of extended CCT in the power system.

In general, there are two methods in obtaining the system CCT: direct method and indirect method [14]–[17]. From direct methods, a specific value of the CCT can be obtained. In the indirect method, the CCT can be found by a process of trial and error in time domain simulation. In this paper, an indirect method was used to determine the system CCT properly in a dynamic simulation environment. The CCT is found by adjusting fault duration time with a several-millisecond interval until the system is able to return to stable state. Thus, the CCT can be obtained as the maximum value with milliseconds-scale error.

A. DETERMINATION OF THE CCT

The CCT is defined as the time taken to reach critical clearing angle, δ_c , from the power angle at a fault inception, δ_0 [18]. It is considered as the fault clearing time at which the system becomes stable after the fault clearance. Thus, faults should be cleared before δ reaches δ_c ; otherwise, the applicable generator becomes unstable.

Fig. 1 shows a P - δ curve and rotor flux dynamics of a SG for a short circuit. During steady state, rotor flux and stator flux rotates at a synchronous speed maintaining an initial power angle, δ_0 , between them. During the fault: the section from Point A to Point C in the P - δ curve, the angular velocity of rotor flux, ω_r , accelerates; thereby, δ increases from δ_0 to δ_1 . In this stage, the kinetic energy of the rotating mass increases.

After the fault is cleared at δ_1 the electrical output, P_e , is restored and δ continues to increase until ω_r becomes equal to the angular velocity of stator flux, ω_s . If ω_r becomes equal to ω_s and P_e is equal to the mechanical input, P_m , then the SG is critically stable. The power angle at Point C, δ_1 , is δ_c in this case. If ω_r becomes equal to ω_s at Point E' in the P - δ curve where P_m is larger than P_e , then there is the acceleration that makes δ increase and the SG never return to steady state.

From the definition of the CCT, it can be directly obtained from δ_c [19]. δ_c can be calculated by equal area criterion knowing P_m , the maximum electrical power, P_{emax} , and δ_0 . δ_c is given by:

$$\cos(\delta_c) = \frac{P_m}{P_{emax}} (180 - 2\delta_0) - \cos(\delta_0). \quad (1)$$

The CCT, t_c , can be obtained by:

$$t_c = \sqrt{2 \frac{M}{P_{acc}} (\delta_c - \delta_0)} \text{ for } \delta_0 < \delta < \delta_c \quad (2)$$

where

$$P_{acc} = P_m - P_e - P_{IBSC} \quad (3)$$

Thus, t_c can be rewritten by:

$$t_c = \sqrt{2 \frac{M}{P_m - P_e - P_{IBSC}} (\delta_c - \delta_0)} \text{ for } \delta_0 < \delta < \delta_c \quad (4)$$

where M and P_{acc} are moment of inertia of the machine and accelerating power, respectively. For normal operations, P_{acc} is definitely equal to zero. However, if there is a fault that causes any mismatch between P_m and P_e , then P_{acc} (excluding P_{IBSC}) is not zero anymore and this changes position of δ . Thus, with an IBSC, P_{IBSC} in (4) reduces P_{acc} to extend the CCT. P_{IBSC} depends on system conditions and a control scheme for the IBSC. Effectiveness of each control scheme will be explored in Case Studies section.

B. EFFECT OF IBSCS ON THE CCT IN POWER SYSTEMS WITH HIGH PENETRATION LEVEL OF IBRSS

There is a mismatch between P_m and P_e of the SG when the SG experiences a fault. The mismatch causes the acceleration of the SG, which is corresponding to Area₁ in Fig. 1(a). Area₁ is determined by the fault clearing time. If the fault is cleared after clearing time, t_c , then the SG becomes unstable and it can cause loss of synchronism in the system. This instability is likely to occur in the power system with a high penetration level of IBRSs because of the difficulty in clearing the fault before t_c and the reduced system inertia. Thus, to compensate for this vulnerability, fast-reacting devices such as an IBSC can be deployed in the system.

IBSCs can be utilized to balance Area₁ and Area₂ by extending the CCT. To do this, an IBSC can be controlled as a variable load near the SG to manipulate the output power of the SG by:

$$2H \frac{1}{\omega_r} \frac{d\omega_r}{dt} = P_m - (P_e + P_{IBSC}) \quad (5)$$

where P_{IBSC} and H are the output of the IBSC and the inertia constant of the SG, respectively.

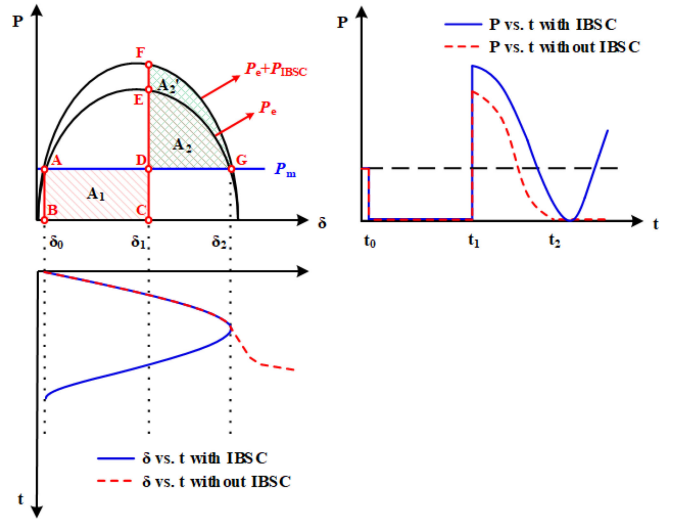


FIGURE 2. Modified P - δ curve of a SG with an IBSC for a short circuit.

In (5), P_{IBSC} can provide two functions to extend the CCT. During a fault, the IBSC can decrease Area₁ by increasing the total load in (5). After the fault clearance, the IBSC can increase Area₂ and reduce the oscillations of the SG by increasing the total load with an anti-oscillation term in (5). Note that the anti-oscillation term is used to mitigate the oscillations caused by interactions among the SGs in the system with the reduced inertia.

Fig. 2 shows the modified P - δ curve with the utilization of an IBSC that helps the angle stability of a synchronous generator by manipulating the electric output. Using clearing fault at δ_1 , a system without IBSC shows that the area A-B-C-D is much larger than area D-E-G. It means that there is an imbalance area between acceleration and deceleration, and as a result, the speed deviation is not equal to zero. Thus, the rotor experiences an acceleration, and the generator will loss of synchronism. However, the proposed method using IBSC shows that the acceleration area A-B-C-D is equal to area D-F-G, which make the system remain stable after clearing at δ_1 . Furthermore, the power waveform without IBSC shows that the generator will lose synchronism, which turns to zero. However, the power waveform with IBSC is oscillated and remain stable. So, it can be concluded that IBSC can extend the critical clearing angle or critical clearing time. Moreover, the power oscillation can be assumed in the time domain as follows:

$$P_{oscillation} = M \cos(\omega t) \quad (6)$$

where M and ω are certain magnitude and the frequency of the oscillation, respectively. Thus, to mitigate $P_{oscillation}$, an IBSC system can employ a droop or speed damping control considering $P_{oscillation}$. If it uses a droop control, then the IBSC system will generate compensating power which has a phase difference of 180 degrees from $P_{oscillation}$. Or, if the IBSC system uses a speed damping control with a washout

filter, then the compensating power will oscillate with a phase difference of 90 degrees from $P_{oscillation}$.

During the zero voltage it is difficult to deliver active power into the power system. Thus, it might be better to inject reactive power during this period to boost the voltage and active power. The IBSC has the potential to reduce the gap between P_e and P_m of a SG during a fault and after the fault clearance; also, the oscillations among SGs can be reduced after the fault clearance. Thus, the utilization of an IBSC can help extend the CCT in a power system where the penetration level of IBRSs is high. To figure out the utilization of an IBSC, proper control schemes of an IBSC are explored in the next section.

Electrical Energy Storage can be stored in different energy forms. According to the stored energy forms, energy storage can be classified into electromagnetic, mechanical, chemical, electro-chemical, thermal, etc. The example of electromagnetic energy storage is supercapacitor energy storage (SC) and superconducting magnetic energy storage (SMES). Mechanical energy storage can be divided into pumped hydro storage, compressed air energy storage, and flywheel energy storage. The example of chemical energy storage is the fuel cell and synthetic natural gas. The battery energy storage system, such as secondary batteries and flow batteries are the example of electro-chemical energy storage. The thermal energy storage, such as cryogenic energy storage still under development [20]–[22].

The response time and ramp rate capability are the main issues in improving power quality. The storage with fast response and small energy capacity is used to enhance system stability. Supercapacitor energy storage is the potential option because it has high power density storage for smoothing high-frequency fluctuation [20]–[22]. Moreover, the supercapacitor has a faster charging and discharging time than batteries in general, which is in accordance with the transient stability time. Thus, after a disturbance happens, the supercapacitor will directly absorb or supply the required power.

The supercapacitor has an extremely high power density rather than the superconducting magnetic energy storage. It also has fast charging and discharging due to its extraordinarily low inner resistance. The supercapacitor has high reliability, durability, long lifetime, no maintenance, and it can be operated over a wide temperature range. Supercapacitor would be effective for applications that reside in remote sites, where maintenance is impractical or even impossible. A supercapacitor is easily recycled and environmentally friendly. Moreover, the efficiency of the supercapacitor is around 75–95%, and the discharge time is in the range of second to hours. Table 1 shows the comparison of energy storage [20], [21].

III. UTILIZATION OF AN IBSC

The proposed utilization of an IBSC with the aim of extending CCT if the power system can be explained as follows. Scheme #1 is activated by comparing the output from a SG with its rated power. When the power exceeds the rated power, the IBSC activates a selected control scheme. Scheme #2 is activated by comparing the rotor speed of a SG with its initial

TABLE 1. Comparison of Electromagnetic Energy Storage

Characteristics	Li-ion	SC	SMES
\$ (kW)	1,200-4,000	100-300	200-300
\$ (kW h)	600-2,500	300-2,000	1,000-10,000
\$ (kW h-per cycle)	15-100	2-20	-
Power rating (MW)	0-0.1	0-0.3	0.1-10
Discharge time typical	min-h	ms-1h	ms-8s
Power density (W/l)	1,300-10,000	100,000	1,000-4,000
Energy density (W h/l)	200-400	10-30	0.2-2.5
Response Time	<s	<s	<s
Efficiency (%)	65-75	85-98	75-80
Self-discharge per day (%)	0.1-0.3	20-40	10-15
Lifetime in years	5-15	> 20	> 20
Lifetime in cycles	1,000-10,000	100,000	100,000

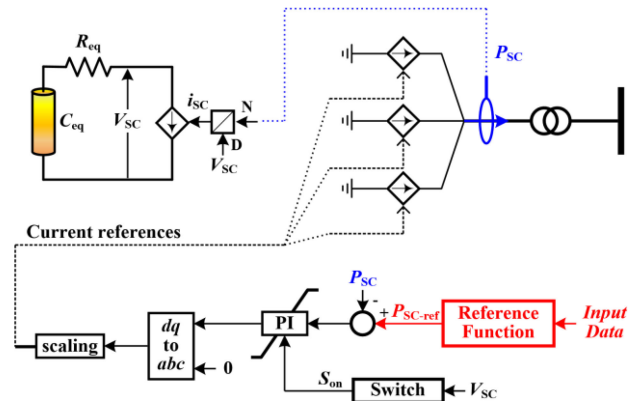


FIGURE 3. Configuration of the simplified IBSC.

speed during the fault. When the frequency of the system exceeds the rated frequency, the IBSC activates the Scheme #2. Moreover, Scheme #3 is a combination between Schemes #1 and #2. It activated when the power and the frequency exceeds its rated value. To do this, the model of the IBSC used in the paper, control scheme, and locations of the IBSC are explained as follows.

A. MODEL OF IBSC

Fig. 3 shows the configuration of a simplified IBSC used in the paper. The simplified IBSC was implemented based on the models described in [23], [24]. The simplified IBSC consists of a bank of SCs, a current-controlled source, and a control system.

The bank of SCs can be represented by its equivalent capacitance, C_{eq} , and resistance, R_{eq} . Detailed descriptions for SC dynamics are described in [24]. In the bank of SCs, the current flow, i_{sc} , is obtained by:

$$i_{sc} = \frac{P_{sc}}{V_{sc}} \quad (7)$$

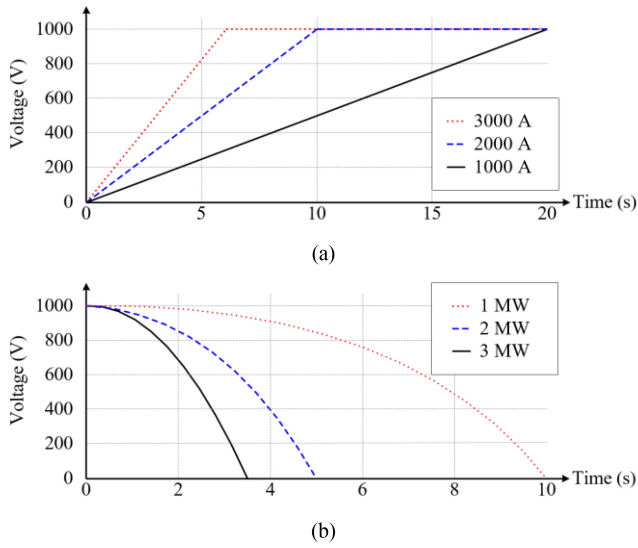


FIGURE 4. Characteristics of the IBSC used in the paper. (a) Voltage rise for a 20-F. (b) Voltage decay for a 20-F [24].

where P_{SC} and V_{SC} are the output power of the IBSC and the voltage at the terminal of the bank, respectively. Fig. 4 shows the characteristics of the SC used in the paper. It shows the voltage rise and the voltage decay for a 20-F IBSC.

The control system of the IBSC processes the power reference, P_{SC-ref} , from a reference function through a proportional-integral controller. Then a current reference is obtained to meet P_{SC-ref} at the terminal of the IBSC. In addition, the operation of the IBSC is terminated by an on-off signal, S_{on} . It is obtained by:

$$S_{on} = \begin{cases} 1, & V_{max} < V_{SC} < V_{min} \\ 0, & \text{otherwise} \end{cases} \quad (8)$$

where V_{max} and V_{min} are the maximum and minimum voltages of the bank, respectively.

B. UTILIZATION OF IBSC

This subsection describes control schemes of an IBSC for extending the CCT, as described in Fig. 2. To achieve this, there are three schemes: Power-damping, speed-damping, and power and speed damping controls.

The vulnerable main generator is apt to lose its synchronism when a fault happens. Thus the IBSC will be located near it. Then, the IBSC can be strongly coupled with an applicable SG electrically, thereby helping extend the CCT with the control schemes.

1) SCHEME #1: POWER-DAMPING CONTROL

The purpose of the scheme is to mitigate output oscillations from a SG by providing the active power that is inverted from the oscillations. This power damping reference, P_{ref-1} , can be obtained by:

$$P_{ref-1} = k_p (P_{pre} - P_{SG}) \quad (9)$$

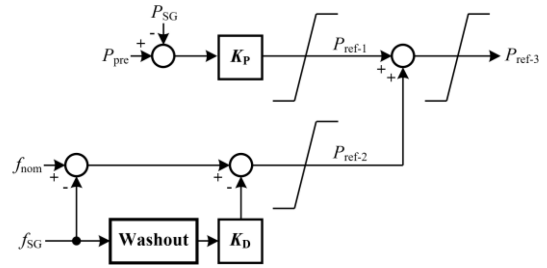


FIGURE 5. Control scheme used in this paper.

where k_p , P_{pre} , and P_{SG} are a proportional constant, pre-fault power of a SG, and active power of a SG, respectively. In this paper, k_p is set to '1'.

Thus, with Scheme #1, the swing equation in (5) can be rewritten by:

$$2H \frac{1}{\omega_r} \frac{d\omega_r}{dt} = P_m - (P_e + P_{ref-1}). \quad (10)$$

2) SCHEME #2: SPEED-DAMPING CONTROL

The purpose of the scheme is to mitigate speed oscillations from a SG by providing the active power that is inverted from its frequency oscillations. This speed damping reference, P_{ref-2} , can be obtained by:

$$P_{ref-2} = k_s (f_{nom} - f_{SG}) - k_D \frac{df_{SG}}{dt} \quad (11)$$

where k_s , k_D , f_{SG} , and f_{nom} are a proportional constant, derivative constant, frequency of SG, and nominal frequency, respectively.

Thus, with Scheme #2, (5) can be rewritten by:

$$2H \frac{1}{\omega_r} \frac{d\omega_r}{dt} = P_m - (P_e + P_{ref-2}). \quad (12)$$

3) SCHEME #3: POWER AND SPEED DAMPING CONTROL

The purpose of the scheme is to mitigate the oscillations in power and speed of a SG by combining Schemes #1 and #2.

This power and speed damping reference, P_{ref-3} , can be obtained by:

$$P_{ref-3} = P_{ref-1} + P_{ref-2}. \quad (13)$$

Thus, with Scheme #3, (5) can be rewritten by:

$$2H \frac{1}{\omega_r} \frac{d\omega_r}{dt} = P_m - (P_e + P_{ref-1} + P_{ref-2}). \quad (14)$$

The best result of the IBSC power output will be examined by implementing all of the schemes in the system. By using the proper scheme, it will give a better performance of IBSC. As a result, the system remains stable after a fault happens, indicated by the extended CCT.

Fig. 5 shows Schemes #1 to #3. In Scheme #1, SG's active power is compared with the pre-fault power of the SG. After that, the error will be multiplied with a proportional gain and limit the power reference. Scheme #2 uses the difference

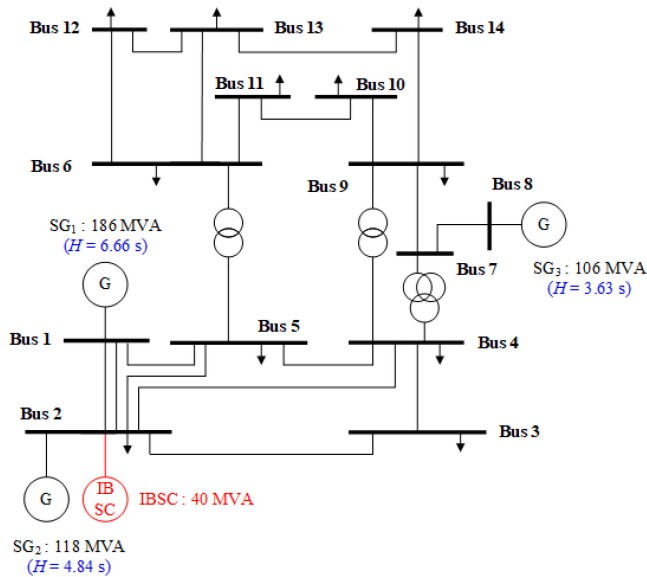


FIGURE 6. Modified IEEE 14-Bus system.

between nominal frequency and the frequency obtained from the SG’s angular speed. A washout filter and the derivative controller are used in this process. Furthermore, Scheme #3 is a combination of Scheme #1 and Scheme #2. An IBSC placed at a certain bus detects the fault and activates a selected control scheme among the three as an active damper.

IV. CASE STUDIES

To explore the utilization of an IBSC (indicated in red) in extending the CCT, a test system, shown in Fig. 6, was modeled. The line parameter values in the test system are taken from the built-in governor and turbine models in PSCAD. The test system consists of three synchronous power plants (SPPs), static loads, and a 40-MVA IBSC. The specific series-parallel arrangement of SCs cells and modules highly depend on the specifications of the cells and modules, which might be different among manufacturers. Hence, in this study, the SC bank is simplified as a single capacitor as shown in the Fig. 3. PSCAD include the machine dynamics, such as alternator and exciter, network dynamics, and the dynamic converter controller. However, during the transient stability study, the dynamics of the transmission network and the stator of the synchronous machines will be neglected [25], [26]. In this study, the case studies were conducted by considering a symmetrical three-phase fault in the system with respect to different system inertia, the control schemes for the IBSC mentioned in Subsection III-B, and fault locations.

For the SPPs, a thermal power plant model was used, and the corresponding thermal governor and turbine models are shown in Figs. 7 and 8; also, the governor and the turbine’s modeling parameters are provided in Table 2.

SG1 is the grid reference because it has the biggest capacity and generation power. Furthermore, the fault is located at the Bus SG1 because of the closer the fault from the main system,

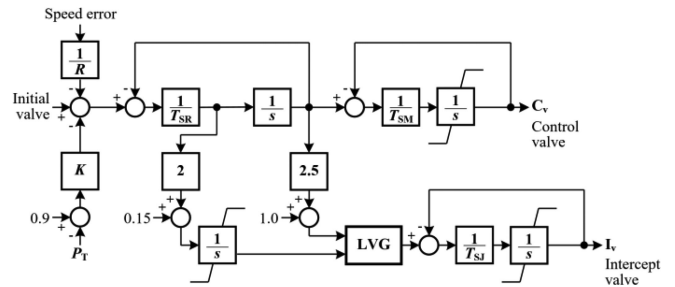


FIGURE 7. Steam governor used in the paper.

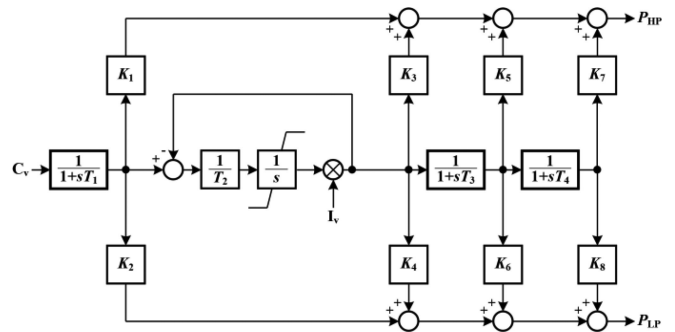


FIGURE 8. Steam turbine used in the paper.

TABLE 2. Test System Parameters

	Parameter		Symbol	Value
	Governor	Permanent droop		R
IV servo time constant		T_{SJ}	0.2 s	
Gate servo time constant		T_{SM}	0.2 s	
Speed relay lag time constant		T_{SR}	0.1 s	
Turbine	i_{th} fraction		K_i	0.125 p.u.
	Steam chest time constant		T_s	1.0 s
	Reheater time constant		T_R	1.0 s
	Reheater/cross-over time constant		T_{RC}	1.0 s
	Cross-over time constant		T_C	1.0 s
	H_i (s)	H_g (s)	H_t (s)	Capacity (MVA)
SG ₁	6.66	2.00	4.66	186
SG ₂	4.84	1.45	3.39	118
SG ₃	3.63	1.09	2.54	106

the less the stability system. Therefore, to simulate severe cases, a fault is located at Bus 1 in each case.

A. EFFECT OF POWER SYSTEM PARAMETERS

The system stability between with and without IBSC is compared using the omega vs. delta, as depicted in Fig. 9. The on-fault point represented by the black dot. From the result, the system without IBSC goes unstable, which is indicated using a red line. However, a system with IBSC represented by

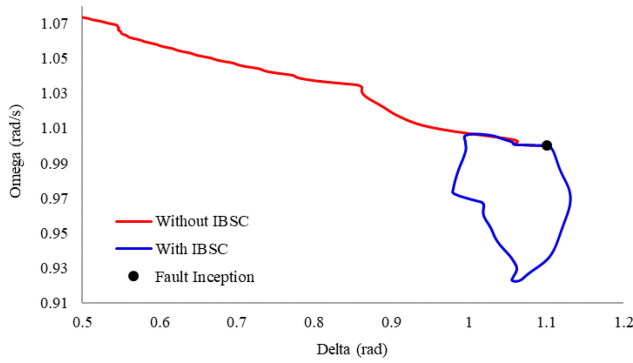


FIGURE 9. Stability system without IBSC vs. with IBSC.

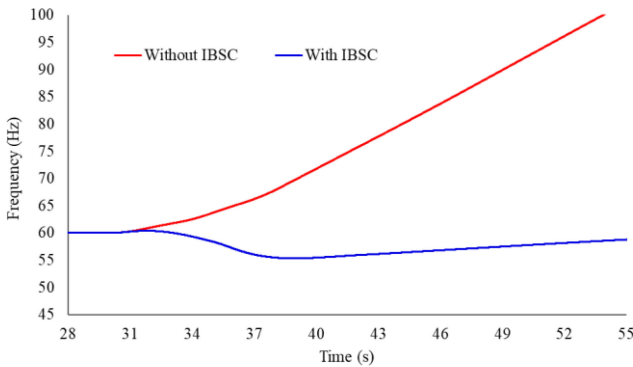


FIGURE 10. System frequencies without IBSC vs with IBSC.

the blue line shows that it goes back to its stable equilibrium point after a fault occurs at 30 s.

Fig. 10 shows the difference in frequency response between the baseline system, which has no IBSC, and the system with IBSC. The baseline system frequency indicated using a red line, and the blue line shows the system with IBSC. The fault occurs at 30 s and lasts for 0.29 s. The system without the IBSC becomes unstable after the fault clearance. On the other hand, the system with IBSC enables the system to secure its stability for the fault.

To explore the effect of different levels of IBRSs’ penetration into a power system on the CCT, the total inertia of the test system of IBRS is reduced from the baseline inertia in Table 2. Furthermore, the system parameter to check the effect of different levels of IBRS’s penetration is the baseline system, which has no IBSC in the system.

There are three groups of generators, which notated by SG_1 , SG_2 , and SG_3 . The total inertia of each group is reduced to evaluate the effect of different inertia constant on CCT. The total inertia is reducing because of the lower power generation of IBRSs. Figs. 11 and 12 show the comparison of the different inertia constant in the test system. There are five cases with different inertia system, case A, case B, case C, case D, and case E. Case A is the system with the highest inertia system, and the inertia time constant is reduced until case E. The inertia time constant of each system are shown in Fig. 12.

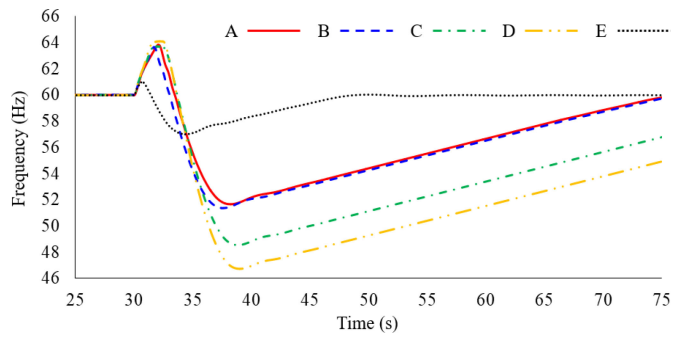


FIGURE 11. System frequencies with different inertia constant.

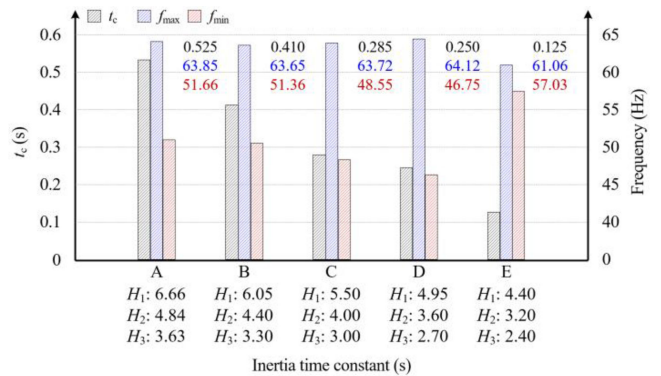


FIGURE 12. Effect of different inertia constant on CCT.

Based on IEEE Std. C37.106-2003, the operational limits for a steam turbine is between 58.5 Hz and 57.9 Hz. This condition is permitted for ten minutes before the turbine blade is damage. However, during the transient condition before 30 cycles, the frequency can operate under 56 Hz [27].

Along with the decrease of inertia constant, the CCT will also decrease. It means the high penetration of IBRSs’ will reduce the robustness of the system. The lower inertia system will make the system more dynamic when a fault happens. Extending the CCT can be one of the options to make the system have more time to maintain its stability when a fault happens.

B. EFFECT OF CONTROL SCHEMES OF IBSC

In order to evaluate the effect of IBSC with respect to the transient stability of the power system, the three control schemes are studied here. Scheme #1 uses power as a damping reference, scheme #2 uses speed as a damping reference, and scheme #3 is the combination of scheme #1 and #2. Three control schemes are compared to know best-proposed control schemes.

As studied in Section IV-A, the inertia constant of case C with the clearing time is 0.285s is used to validate the control schemes. A three-phase short circuit happens at $t = 30$ s, and new CCT is obtained for each control scheme, as shown in Table 3. It can be observed that Scheme #1 presents higher

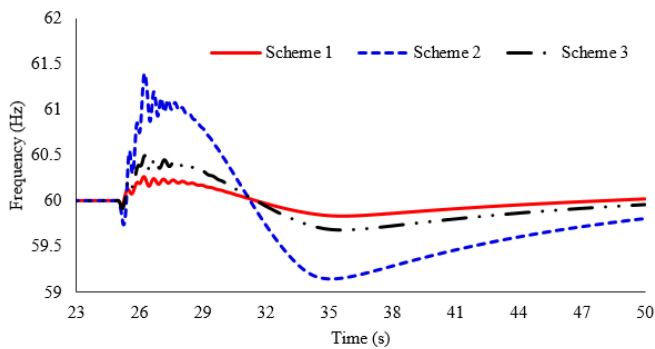


FIGURE 16. System frequencies for each control scheme in distribution system.

schemes show a good response when a fault happens. The IBS is absorbing the excess power from the SG. The frequency nadir of the system is different among each scheme. Scheme #1 is 59.83 Hz, Scheme #2 is 59.14 Hz, and Scheme #3 59.67 Hz. Moreover, the highest frequency of the system using Scheme #1 is 60.26 Hz, while Scheme #2 and Scheme #3 are 61.39 Hz and 60.49 Hz, respectively. From the simulation in the distribution system, it can be concluded that the control schemes are work properly not only in the transmission system. Furthermore, control Scheme #1 shows a better result more than Scheme #2 and Scheme #3.

V. CONCLUSION

Transient stability limit is one of the main aspects in the power system. Furthermore, in the near future, the system will have a high penetration level of IBRSs. In this paper, the effect of high penetration of the IBRSs system is modeled as a smaller inertia system. The result shows that more penetration of IBRSs will reduce system stability.

Furthermore, this paper proposes the utilization of IBSC to extend the CCT of the power system with a high penetration level of IBRSs. Three control schemes are proposed to utilize the IBSC, which are power-damping control, speed-damping control, and a combination of power-damping control. Furthermore, the proposed control schemes are validated in the transmission system and the distribution system.

The simulation result shows that the IBSC with power-damping control and located at the main generator, which is vulnerable when a fault happens, provides better stability. It is shown by the response of system frequency and the extending of the CCT value. Thereby, the proposed method can help secure the system stability of a power system with high penetration of IBRSs. Although the proposed method can perform well in the PSCAD with various cases, further study is necessary to implement the proposed method in the power network. Thus, the authors have invited all the researchers to implement the proposed method in the near future.

ACKNOWLEDGMENT

The author would like to thank Kementerian Riset, Teknologi dan Pendidikan Tinggi Republik Indonesia (Kemristekdikti

RI), Institut Teknologi Sepuluh Nopember Indonesia (ITS) and Auburn University for providing facilities and support this work through Enhancing International Publication Program-PMDSU scholarship.

REFERENCES

- [1] A. A. Almezhia, H. M. K. Al-Masri, and M. Ehsani, "Feasibility study of sustainable energy sources in a fossil fuel rich country," *IEEE Trans. Ind. Appl.*, vol. 55, no. 5, pp. 4433–4440, Sep. 2019.
- [2] K. Handayani, Y. Krozer, and T. Filatova, "From fossil fuels to renewables: An analysis of long-term scenarios considering technological learning," *Energy Policy*, vol. 127, pp. 134–146, Apr. 2019.
- [3] S. Eftekharijad, V. Vittal, G. T. Heydt, B. Keel, and J. Loehr, "Impact of increased penetration of photovoltaic generation on power systems," *IEEE Trans. Power Syst.*, vol. 28, no. 2, pp. 893–901, May 2013.
- [4] "Massive blackout hits tens of millions in South America," AP NEWS, Jun. 17, 2019. Accessed: Apr. 16, 2020. [Online]. Available: <https://apnews.com/a29b1da1a91542faa91d68cf8e97a34d>.
- [5] A. Beo Da Costa and G. Suroyo, "Power restored to some areas in Indonesia capital, parts of Java after 9 hours," Reuters, Aug. 4, 2019. [Online]. Available: <https://www.reuters.com/article/us-indonesia-power-idUSKCN1UU060>
- [6] H. Kang, Y. Liu, Q. H. Wu, and X. Zhou, "Switching excitation controller for enhancement of transient stability of multi-machine power systems," *CSEE J. Power Energy Syst.*, vol. 1, no. 3, pp. 86–93, Sep. 2015.
- [7] Y. Liu, Q. H. Wu, H. Kang, and X. Zhou, "Switching power system stabilizer and its coordination for enhancement of multi-machine power system stability," *CSEE J. Power Energy Syst.*, vol. 2, no. 2, pp. 98–106, Jun. 2016.
- [8] J. V. Milanovic and I. A. Hiskens, "Effects of load dynamics on power system damping," *IEEE Trans. Power Syst.*, vol. 10, no. 2, pp. 1022–1028, May 1995.
- [9] A. Kanchanaharuthai, V. Chankong, and K. A. Loparo, "Transient stability and voltage regulation in multimachine power systems Vis-à-Vis STATCOM and battery energy storage," *IEEE Trans. Power Syst.*, vol. 30, no. 5, pp. 2404–2416, Sep. 2015.
- [10] I. Ngamroo and S. Vachirasricirikul, "Optimized SFCL and SMES units for multimachine transient stabilization based on kinetic energy control," *IEEE Trans. Appl. Supercond.*, vol. 23, no. 3, pp. 5000309–5000309, Jun. 2013.
- [11] M. R. Hossain, M. K. Hossain, M. H. Ali, Y. Luo, and R. Hovsapian, "Synchronous generator stabilization by thyristor controlled supercapacitor energy storage system," in *IEEE SoutheastConf. 2017*, Mar. 2017, Charlotte, NC, USA, pp. 1–6.
- [12] I. Kiaei and S. Lotfifard, "Tube-based model predictive control of energy storage systems for enhancing transient stability of power systems," *IEEE Trans. Smart Grid*, vol. 9, no. 6, pp. 6438–6447, Nov. 2018.
- [13] *PSCAD Power System Simulation User, Guide*, EMTDC TM, Manitoba HVDC Research Centre.
- [14] N. Yorino, A. Priyadi, H. Kakui, and M. Takeshita, "A new method for obtaining critical clearing time for transient stability," *IEEE Trans. Power Syst.*, vol. 25, no. 3, pp. 1620–1626, Aug. 2010.
- [15] T. L. Vu, S. M. A. Araifi, M. S. E. Moursi, and K. Turitsyn, "Toward simulation-free estimation of critical clearing time," *IEEE Trans. Power Syst.*, vol. 31, no. 6, pp. 4722–4731, Nov. 2016.
- [16] T. P. Sari, A. Priyadi, M. Pujiyantara, N. Yorino, and M. H. Purnomo, "Improving transient stability assessment by installing super capacitor energy storage using critical trajectory method based on modified losing synchronism," *Int. Seminar Intell. Technol. Appl.*, Aug. 2018, pp. 51–55.
- [17] A. Priyadi, T. P. Sari, I. Hafidz, M. Pujiyantara, N. Yorino, and M. H. Purnomo, "Losing synchronism technique based on critical trajectory method for obtaining the CCT with installing SCES," *Int. Seminar Intell. Technol. Appl.*, Aug. 2018, pp. 63–66.
- [18] A. R. Bergen, *Power System Stability Analysis*. New York, NY, USA: McGraw-Hill, 1994.
- [19] W. D. Stevenson, *Elements of power system analysis*. New York, NY, USA: McGraw-Hill, 1982.

- [20] D. O. Akinyele and R. K. Rayudu, "Review of energy storage technologies for sustainable power networks," *Sustain. Energy Technol. Assess.*, vol. 8, pp. 74–91, Dec. 2014.
- [21] H. Zhao, Q. Wu, S. Hu, H. Xu, and C. N. Rasmussen, "Review of energy storage system for wind power integration support," *Appl. Energy.*, vol. 137, pp. 545–553, Jan.
- [22] Y. Cho and H. A. Gabbar, "Review of energy storage technologies in harsh environment," *Saf. Extreme Environ.*, vol. 1, no. 1, pp. 11–25, Dec. 2019.
- [23] V. Gevorgian, E. Muljadi, Y. Luo, M. Mohanpurkar, and R. Hovsapien, and V. Koritarov, "Supercapacitor to provide ancillary services," *IEEE Energy Convers. Congr. Expo.*, Cincinnati, OH, USA, Oct. 2017, pp. 1030–1036.
- [24] J. Kim, V. Gevorgian, Y. Luo, M. Mohanpurkar, V. Koritarov, and R. Hovsapien, "Supercapacitor to provide ancillary services with control coordination," *IEEE Trans. Ind. Appl.*, vol. 55, no. 5, pp. 5119–5127, Sep./Oct. 2019.
- [25] P. M. Anderson and A. A. Fouad, *Power System Control and Stability*, New-York: IEEE Press, 1994.
- [26] F. Milano, *Advances in Power System Modelling, Control and Stability Analysis*. London, U.K.: Institution of Engineering and Technology, 2016.
- [27] "IEEE guide for abnormal frequency protection for power generating plants," IEEE Standard C37.106-2003 Revis. ANSI IEEE C37.106-1987, pp. 1–34, 2004.



VITA LYSTIANINGRUM (Member, IEEE) received the B.S. degree in electrical engineering from the Institut Teknologi Sepuluh Nopember (ITS), Indonesia in 2005, the M.S. degree from Hochschule Darmstadt, Darmstadt, Germany in 2007, and the Ph.D. degree from the University of New South Wales in 2016. She is currently a Lecturer with Electrical Engineering Department, ITS. Her research interest is energy storage monitoring and diagnostics.



MAURIDHI HERY PURNOMO (Senior Member, IEEE) received the B.S. degree from the Electrical Engineering Institut Teknologi Sepuluh Nopember (ITS), Surabaya in 1984, the M.S. degree in 1989 and the Ph.D. degree from the Electrical Engineering Osaka City University, Japan in 1995. He is a Professor with the ITS and involved in teaching on research philosophy, artificial intelligence, neural network, and image processing. His research interests include smart grid, renewable energy, artificial intelligent application on healthcare and power

systems. He is the Chair of the IEEE Industrial Electronics Society Indonesia Section.



TALITHA PUSPITA SARI (Student Member, IEEE) received the B.S. degree in electrical engineering, from Institut Teknologi Sepuluh Nopember (ITS), in 2017. She is currently working toward the Ph.D degree with Institut Teknologi Sepuluh Nopember. She was an Erasmus Awardee in Anadolu University and a Visiting Scholar working in collaboration with Auburn University. Her research interest include transient stability, protection system, supercapacitor energy storage, and artificial intelligence application in power systems.



EDUARD MULJADI (Fellow, IEEE) received the Ph.D. degree in electrical engineering from the University of Wisconsin, Madison, WI, USA, in 1987. He was a Faculty with the California State University, Fresno, CA, USA, from 1988 to 1992. From 1992 to 2017, he was with the National Renewable Energy Laboratory, Golden, CO, USA. And, in January 2018, he was with Auburn University, Auburn, AL, USA, as the James J. Danaher Distinguished Professor. He holds patents in power conversion for renewable energy. His research interests include electric machines, power electronics and power systems, and renewable energy. Dr. Muljadi is a Member of Eta Kappa Nu and Sigma Xi, and an Editor for the IEEE TRANSACTIONS ON ENERGY CONVERSION. He is a Member of various subcommittees within the IEEE Industry Application Society, Power Electronics Society, and Power and Energy Society (PES). He is a Founding Member and the past Chair of Renewable Energy Machines and Systems and the Chair of the Advanced Pumped Storage Hydropower Modeling Task Force within the PES.

Dr. Muljadi is a Member of Eta Kappa Nu and Sigma Xi, and an Editor for the IEEE TRANSACTIONS ON ENERGY CONVERSION. He is a Member of various subcommittees within the IEEE Industry Application Society, Power Electronics Society, and Power and Energy Society (PES). He is a Founding Member and the past Chair of Renewable Energy Machines and Systems and the Chair of the Advanced Pumped Storage Hydropower Modeling Task Force within the PES.



JINHO KIM (Member, IEEE) received the B.S., M.S., and Ph.D. degrees in electrical engineering from the Chonbuk National University, Jeonju, South Korea, in 2013, 2015, and 2018, respectively. From 2012 to 2017, he worked on developing voltage and frequency control schemes of a wind power plant. Since 2018, he has been a Postdoctoral Fellow with the Department of Electrical and Computer Engineering, Auburn University, Auburn, AL, USA, and is recently working on the development of voltage and frequency control

schemes of renewable energy applications.



ARDYONO PRIYADI (Member, IEEE) received the B.S. degree in electrical engineering from the Institut Teknologi Sepuluh Nopember (ITS), Indonesia in 1997, M.S. and Ph.D. degrees in electrical engineering from Hiroshima University, Hiroshima, Japan, in 2011. He is currently an Associate Professor with the Electrical Engineering Department, ITS. He is registered as a Professional Engineer (Ir.) in Indonesia. He is experienced in assessing the transient stability of the industrial power system. His research interests include power

system dynamics and control, transient stability, renewable energy, and artificial intelligence application in power systems.